CIRCADIAN RHYTHMS

Rev-erbα dynamically modulates chromatin looping to control circadian gene transcription

Yong Hoon Kim,[1,2,3]* Sajid A. Marhon,[1,2,3]* Yuxiang Zhang,[1,2] David J. Steger,[1,2] Kyoung-Jae Won,[1,2,3]† Mitchell A. Lazar[1,2,3]†

Mammalian physiology exhibits 24-hour cyclicity due to circadian rhythms of gene expression controlled by transcription factors that constitute molecular clocks. Core clock transcription factors bind to the genome at enhancer sequences to regulate circadian gene expression, but not all binding sites are equally functional. We found that in mice, circadian gene expression in the liver is controlled by rhythmic chromatin interactions between enhancers and promoters. Rev-erbα, a core repressive transcription factor of the clock, opposes functional loop formation between Rev-erbα–regulated enhancers and circadian target gene promoters by recruitment of the NCoR-HDAC3 co-repressor complex, histone deacetylation, and eviction of the elongation factor BRD4 and the looping factor MED1. Thus, a repressive arm of the molecular clock operates by rhythmically modulating chromatin loops to control circadian gene transcription.

Circadian rhythms of mammalian physiology are orchestrated by core clock transcription factors (TFs) functioning as activators or repressors in interlocking feedback loops that drive daily oscillations of gene expression (*1*, *2*). These TFs generate circadian rhythms of histone modification at circadian enhancers (*3*–*6*). Enhancer activities are mediated by looping to promoters within insulated topologically associating domains (TADs) (*7*–*9*). Previous studies with cultured cells have described circadian regulation of higher-order chromatin organization (*10*), long-range interchromosomal interactions (*11*), and short-range chromatin loops (*12*) at specific loci, but this has not been examined at a genome-wide level in native tissues under normal physiology.

We performed in situ Hi-C (*13*, *14*) on C57BL/6J mouse livers harvested 12 hours apart, at zeitgeber time 22 (ZT22, 5 a.m.) and ZT10 (5 p.m.), to examine whether chromatin interactions change in a circadian manner. Hi-C identified megabase-size TADs whose boundaries were highly similar to those identified in mouse embryonic stem cells (fig. S1A). This was expected because TADs are largely conserved among different tissues (*7*), and indeed the overall TAD organization was also highly similar between ZT22 and ZT10 (fig. S1B). Within each TAD we also observed submegabase structures (sub-TADs) of different lengths (fig. S1C) that were flanked by CTCF and cohesin (RAD21) and internally occupied by Mediator (MED1) (fig. S1D), as described previously (*14*–*17*). Globally, genomic occupancy of CTCF and cohesin at ZT10 versus ZT22 was very similar at sub-TAD boundaries (fig. S1, E and F).

Because TFs bind at enhancers to regulate genes confined within sub-TAD boundaries (*16*), we next searched for "intra-TAD" interactions occurring within sub-TADs. Of 6510 intra-TAD interactions, only 349 were ZT22-specific, whereas 527 were ZT10-specific (Wilcoxon signed-rank test, $P < 0.001$). For example, the circadian *Npas2* gene exhibited increased intra-TAD interactions at ZT22, including extensive looping between the transcriptional start site and four noncoding regions (E1 to E4) (Fig. 1A). These noncoding regions

[1]Institute for Diabetes, Obesity, and Metabolism, University of Pennsylvania Perelman School of Medicine, Philadelphia, PA 19104, USA. [2]Division of Endocrinology, Diabetes, and Metabolism, Department of Medicine, University of Pennsylvania Perelman School of Medicine, Philadelphia, PA 19104, USA. [3]Department of Genetics, University of Pennsylvania Perelman School of Medicine, Philadelphia, PA 19104, USA.
*These authors contributed equally to this work.
†Corresponding author. Email: wonk@pennmedicine.upenn.edu (K.-J.W.); lazar@pennmedicine.upenn.edu (M.A.L.)

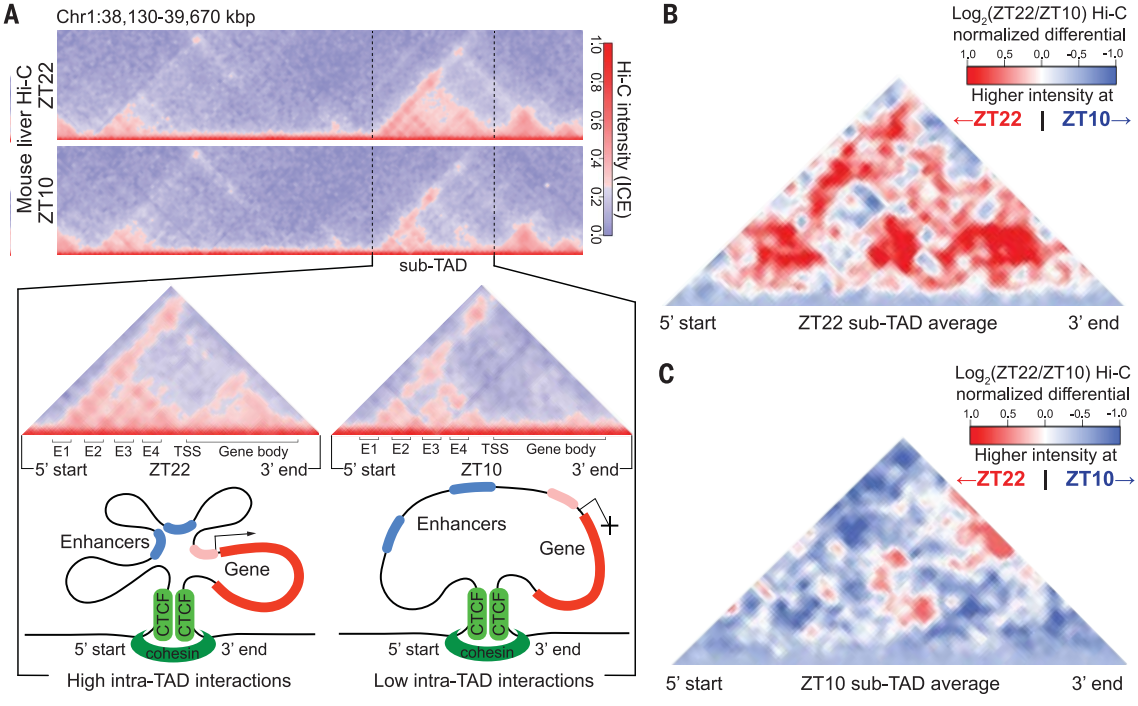

Fig. 1. Circadian sub-TADs undergo rhythmic intra-TAD compaction within stable boundaries. (**A**) Heat maps of ZT22 and ZT10 Hi-C demonstrating circadian intra-TAD interactions within sub-TAD boundaries (dashed lines), as represented by Hi-C intensity normalized by iterative correction and eigenvector decomposition (ICE). The transcriptional start site of the *Npas2* gene (TSS) forms rhythmic intra-TAD loops with upstream enhancers (E1 to E4) as well as with the gene body, as illustrated by schematics below. (**B** and **C**) ZT22 sub-TAD (B) and ZT10 sub-TAD (C) averaged differential changes in intra-TAD interactions visualized as $\log_2$ ratio within size-normalized sub-TAD 5′ and 3′ boundaries (red, higher interaction ratio at ZT22; blue, higher interaction ratio at ZT10).

mapped to regions of divergent transcriptional activity characteristic of enhancer RNA (eRNA) that were similarly regulated (fig. S2A). Intra-TAD interaction was also observed within the gene body, as previously reported at actively transcribed genes (*18*, *19*), and this was enhanced at ZT22 as well (Fig. 1A).

Genome-wide, we identified hundreds of sub-TADs containing circadian genes whose expression has been shown to peak between ZT21 and ZT24 ("ZT22 sub-TADs") or between ZT9 and ZT12 ("ZT10 sub-TADs") (*6*). The overall structure of these sub-TADs (fig. S2B) and the binding of CTCF and RAD21 at their boundaries (fig. S2, C and D) changed very little between ZT22 and ZT10 (fig. S2, B to D). However, ZT22 and ZT10 sub-TADs exhibited greater intra-TAD interactions corresponding to their transcriptional activities (Fig. 1, B and C), whereas noncircadian sub-TADs did not (fig. S3A). Similar conclusions were obtained when the circadian windows were adjusted by 1 hour (fig. S3, B and C). Interactions within gene bodies were also circadian (fig. S3, D to H).

The circadian *Cry1* locus is located within a ZT22 sub-TAD, and Hi-C revealed an interaction between the gene promoter and an intronic enhancer that was increased at ZT22 (fig. S4, A and B), as best visualized by differential analysis of the data (Fig. 2A). The nuclear receptor Rev-erbα, a repressive component of the mammalian clock whose expression peaks at ZT10 to confer circadian expression of genes in the opposite phase (*6*, *20*, *21*), binds at this intronic enhancer (Fig. 2A). The enhancer-promoter (E-P) loop identified in ZT22 Hi-C was confirmed by chromatin conformation capture (3C) experiments (Fig. 2B). Tandem 3C and Rev-erbα chromatin immunoprecipitation (ChIP) at six time points throughout the day revealed that this E-P loop was indeed circadian and in phase with *Cry1* mRNA expression, with a peak that was antiphase to Rev-erbα binding (Fig. 2C). At ZT10, both looping from the Rev-erbα site to the *Cry1* promoter (Fig. 2D) and *Cry1* gene expression (Fig. 2E) were enhanced by knockout (KO) of Rev-erbα, which attenuated the rhythmicity of these parameters over the course of 24 hours (fig. S4C). Reciprocally, ectopic expression of Rev-erbα in liver was sufficient to reduce looping as well as mRNA expression at ZT22 (Fig. 2, F and G), consistent with an active role of Rev-erbα in opposing loop formation. We next performed Hi-C on livers from mice genetically lacking Rev-erbα and harvested at ZT10, which confirmed the enhanced E-P looping at the *Cry1* locus (fig. S4D). Moreover, throughout the genome, intra-TAD interactions that were normally favored at ZT22 were increased in the genetic absence of Rev-erbα at ZT10 (Fig. 2H).

These findings suggested that the ability of Rev-erbα to oppose loop formation is a critical feature at binding sites from which Rev-erbα actively represses transcription. To explore the relationship between regulation of looping and functional repression, we identified Rev-erbα binding sites that directly loop to promoters at ZT22 in the physiological absence of Rev-erbα. E-P loops at Rev-erbα binding sites were defined as "engaged" when transcription of the gene body was repressed at ZT10, or "passive" if not repressed (Fig. 3, A and B). Engaged sites were highly correlated

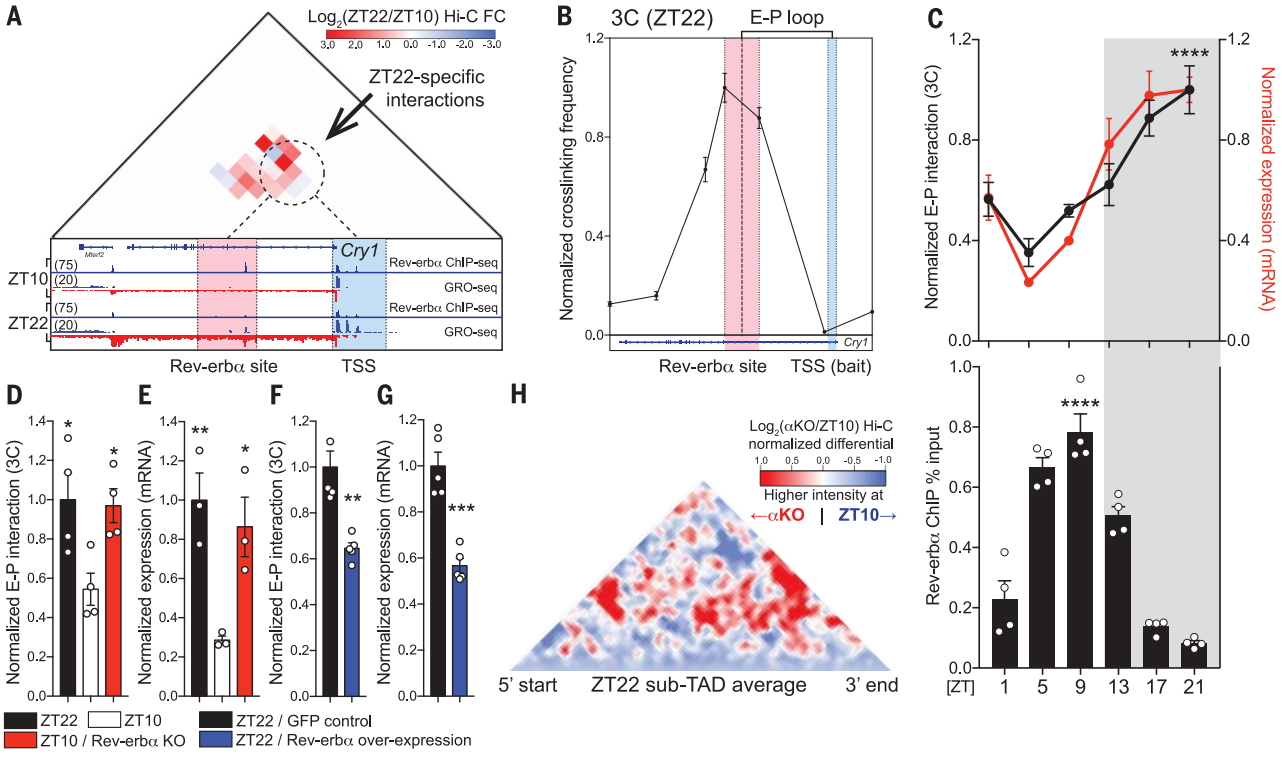

Fig. 2. Rev-erbα causally opposes enhancer-promoter loop formation. (**A**) Differential Hi-C analysis at the *Cry1* locus revealing ZT22-specific interactions, represented as $\log_2$ ratio (ZT22 Hi-C/ZT10 Hi-C). ZT22-specific interactions (dashed circle) occur between a region around the intronic Rev-erbα site (red) and the *Cry1* TSS (blue). Global run-on sequencing (GRO-seq) demonstrates circadian nascent transcription as well as the presence of bidirectional eRNA at the Rev-erbα site at ZT22. (**B**) 3C validation of enhancer-promoter loop (E-P loop) identified at ZT22 between the Rev-erbα site (red) and TSS (blue) (n = 5, mean ± SEM). (**C**) Circadian plot demonstrating *Cry1* E-P loop, mRNA expression, and Rev-erbα ChIP ± SEM [n = 4 or 5, P values shown for 3C and ChIP peaks compared to troughs, one-way analysis of variance (ANOVA) followed by multiple-comparisons correction with the Tukey method]. (**D** and **E**) E-P loop (D) and mRNA expression (E) of *Cry1* at ZT22 (black), ZT10 (white), and ZT10 Rev-erbα knockout (KO) (red), represented as mean ± SEM (n = 4, one-way ANOVA followed by Dunnett multiple-comparisons test). (**F** and **G**) E-P loop (F) and mRNA expression (G) of *Cry1* at ZT22 with control green fluorescent protein (GFP) expression (black) versus Rev-erbα overexpression (blue) expressed as mean ± SEM (n = 5, two-tailed Student t test). (**H**) Same analysis as in Fig. 1B, but comparing ZT10 Rev-erbα KO (αKO) to wild-type ZT10 at ZT22 sub-TADs (red, higher interaction ratio at ZT10 αKO; blue, higher interaction ratio at wild-type ZT10). *P < 0.05, **P < 0.01, ***P < 0.001, ****P < 0.0001.

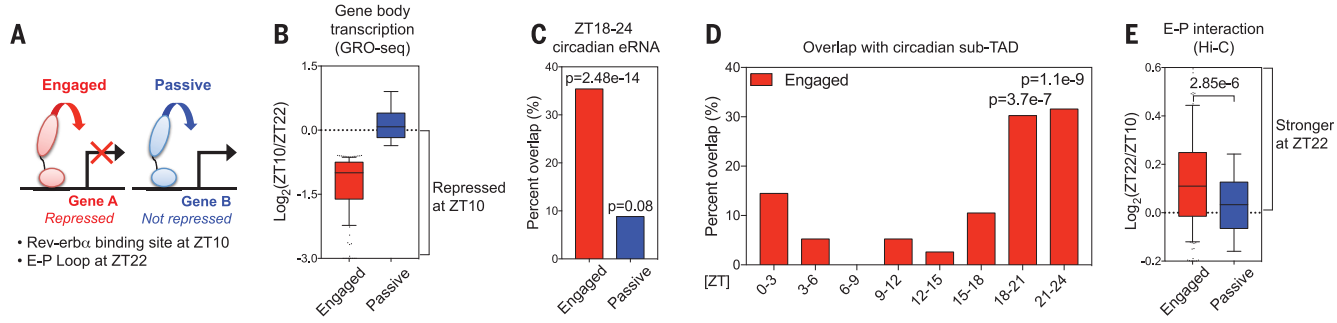

Fig. 3. Rev-erbα attenuates enhancer-promoter looping at functional binding sites. (**A**) Rev-erbα sites at E-P loops were classified as engaged when looped to genes whose transcription was repressed at ZT10 relative to ZT22, and otherwise classified as passive. (**B**) Gene body transcription change between ZT22 and ZT10 at engaged versus passive sites. Engaged target genes were defined as those displaying gene body transcription relative change of ≥1.5 between ZT22 and ZT10. (**C**) Engaged Rev-erbα sites were highly correlated with ZT18-24 circadian eRNAs (*6*) (within ±2 kbp, one-tailed hypergeometric tests). (**D**) Engaged Rev-erbα sites were confined within sub-TADs that contain circadian genes peaking at ZT18-24 (one-tailed hypergeometric tests). (**E**) E-P loops between engaged Rev-erbα binding sites and target gene promoters were stronger at ZT22 than at ZT10 (Mann-Whitney test). For box plots in (B) and (E), whiskers denote the 10th and 90th percentiles.

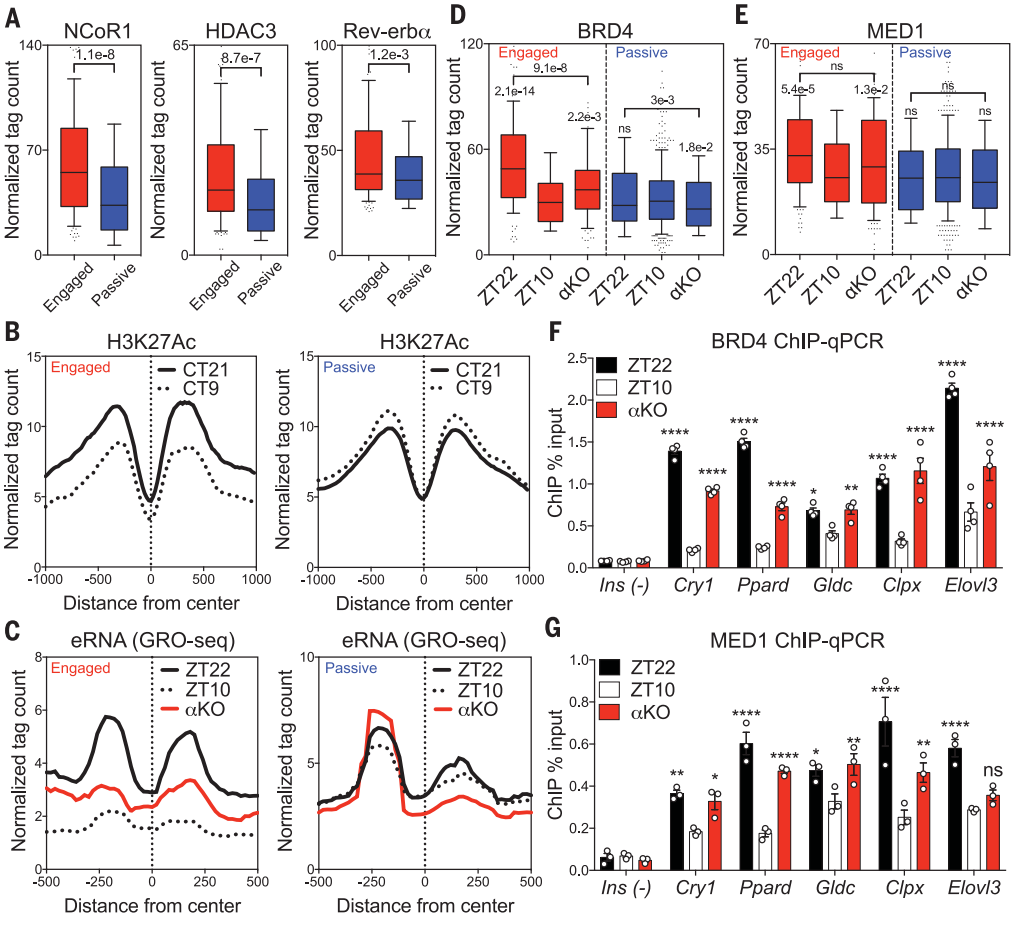

Fig. 4. Functional Rev-erbα binding evicts BRD4 and MED1 from sites of looping. (**A**) Greater recruitment of NCoR1 and HDAC3 at engaged Rev-erbα sites associated with a slight average increase in Rev-erbα binding (Mann-Whitney tests). (**B**) Circadian deacetylation of H3K27Ac at circadian time 21 (CT21) and CT9 at engaged versus passive sites [data sets from (*5*)]. (**C**) Circadian eRNA transcription between ZT22 and ZT10, with increased transcription at ZT10 in αKO at engaged sites [data sets from (*6*)]. (**D** and **E**) Circadian eviction of BRD4 (D) and MED1 (E) between ZT22 and ZT10, with enhanced binding at ZT10 in αKO at engaged sites (Dunn multiple-comparisons tests after one-way ANOVA/Friedman test). (**F** and **G**) ChIP-qPCR validation of BRD4 (F) and MED1 (G) eviction at ZT10 and enhanced binding at ZT10 in αKO at engaged sites (*Ins* as a negative control, $n = 3$ or 4, two-way ANOVA followed by Dunnett multiple-comparisons test). For box plots in (A), (D), and (E), whiskers denote the 10th and 90th percentiles. *$P < 0.05$, **$P < 0.01$, ****$P < 0.0001$; ns, not significant.

with circadian eRNAs whose activity peaked around ZT18 to ZT24 (ZT18-24) antiphase to Rev-erbα binding (Fig. 3C), demonstrating that engaged sites are direct links between circadian eRNAs and genes repressed by Rev-erbα. De novo motif analysis at engaged sites revealed enrichment of DNA motifs known to be bound by Rev-erbα directly (RORE and RevDR2) (*22*) or indirectly (HNF6) (*21*) (fig. S5A), whereas these motifs were not enriched at passive sites (fig. S5B). Although the number of sub-TADs containing circadian genes from each phase was similar (fig. S5C), only engaged Rev-erbα sites were enriched in ZT18-24 circadian sub-TADs (Fig. 3D and fig. S5D). Most important, E-P interactions at engaged Rev-erbα binding sites were strengthened at ZT22 relative to ZT10 (Fig. 3E). Together, these findings show that the ability of Rev-erbα to oppose E-P loops within sub-TADs is a likely determinant of active repression by Rev-erbα.

We next addressed the mechanism by which Rev-erbα binding controls circadian E-P interactions. The repressive action of Rev-erbα is often mediated by recruitment of a co-repressor complex containing NCoR (nuclear receptor co-repressor) and HDAC3 (histone deacetylase 3) (*23*), leading to circadian histone deacetylation associated with repressed enhancers (*3*). Indeed, recruitment of NCoR and HDAC3 was greater at engaged Rev-erbα binding sites, with a modest average increase in Rev-erbα binding relative to passive sites (Fig. 4A). Consistent with this finding, the previously demonstrated circadian acetylation of histone H3 Lys^{27} (H3K27Ac) in mouse liver (*5*) was exaggerated at engaged Rev-erbα binding sites but

was nearly absent at passive sites (Fig. 4B). eRNA transcription also demonstrated an enhanced circadian rhythm at engaged sites, which was abrogated in livers lacking Rev-erbα (Fig. 4C); this finding shows that Rev-erbα was required for the epigenomic rhythms that occurred selectively at engaged sites.

The transcriptional regulator BRD4 acts as a reader of acetylated histone (*24*–*26*) and forms a functional transcriptional complex with the well-established looping factor MED1 (*27*–*30*). In agreement with the changes in H3K27Ac at engaged sites, BRD4 binding was greater at ZT22 than at ZT10, and this difference was attenuated in the genetic absence of Rev-erbα (Fig. 4D). Similarly, MED1 was also evicted at engaged sites but not in livers lacking Rev-erbα (Fig. 4E). The opposition of Rev-erbα to the circadian binding of BRD4 and MED1 was confirmed by ChIP–quantitative polymerase chain reaction (qPCR) in both the genetic absence (Fig. 4, F and G) and ectopic expression of Rev-erbα (fig. S6, A to C). Focusing on Rev-erbα binding sites where BRD4 is evicted at ZT10 (fig. S6D) revealed the concurrent eviction of MED1 (fig. S6E) and also independently predicted functional sites with circadian eRNA transcription (fig. S6F). However, the binding of CTCF and RAD21 was low and not circadian at Rev-erbα binding sites (fig. S6, G to J).

Our findings demonstrate genome-wide organizational plasticity at the level of sub-TADs that occurs in a circadian manner as a component of normal mammalian physiology. The mechanisms by which Rev-erbα functionally opposes E-P loop formation, leading to circadian repression of gene transcription within sub-TADs, are likely applicable to other transcriptional repressors whose function in controlling chromatin architecture is currently not as well defined as for transcriptional activators.

REFERENCES AND NOTES

1. J. Bass, M. A. Lazar, *Science* **354**, 994–999 (2016).
2. J. S. Takahashi, *Nat. Rev. Genet.* **18**, 164–179 (2017).
3. D. Feng *et al.*, *Science* **331**, 1315–1319 (2011).
4. N. Koike *et al.*, *Science* **338**, 349–354 (2012).
5. C. Vollmers *et al.*, *Cell Metab.* **16**, 833–845 (2012).
6. B. Fang *et al.*, *Cell* **159**, 1140–1152 (2014).
7. J. R. Dixon *et al.*, *Nature* **485**, 376–380 (2012).
8. E. P. Nora *et al.*, *Nature* **485**, 381–385 (2012).
9. T. Sexton *et al.*, *Cell* **148**, 458–472 (2012).
10. H. Zhao *et al.*, *Mol. Cell* **59**, 984–997 (2015).
11. L. Aguilar-Arnal *et al.*, *Nat. Struct. Mol. Biol.* **20**, 1206–1213 (2013).
12. Y. Xu *et al.*, *PLOS Genet.* **12**, e1005992 (2016).
13. E. Lieberman-Aiden *et al.*, *Science* **326**, 289–293 (2009).
14. S. S. P. Rao *et al.*, *Cell* **159**, 1665–1680 (2014).
15. J. E. Phillips-Cremins *et al.*, *Cell* **153**, 1281–1295 (2013).
16. J. M. Dowen *et al.*, *Cell* **159**, 374–387 (2014).
17. R. Siersbæk *et al.*, *Mol. Cell* **66**, 420–435.e5 (2017).
18. S. M. Tan-Wong *et al.*, *Science* **338**, 671–675 (2012).
19. A. R. Grosso, S. F. de Almeida, J. Braga, M. Carmo-Fonseca, *Genome Res.* **22**, 1447–1456 (2012).
20. N. Preitner *et al.*, *Cell* **110**, 251–260 (2002).
21. Y. Zhang *et al.*, *Science* **348**, 1488–1492 (2015).
22. H. P. Harding, M. A. Lazar, *Mol. Cell. Biol.* **15**, 4791–4802 (1995).
23. L. Yin, M. A. Lazar, *Mol. Endocrinol.* **19**, 1452–1459 (2005).
24. A. Dey, F. Chitsaz, A. Abbasi, T. Misteli, K. Ozato, *Proc. Natl. Acad. Sci. U.S.A.* **100**, 8758–8763 (2003).
25. J. S. Roe, F. Mercan, K. Rivera, D. J. Pappin, C. R. Vakoc, *Mol. Cell* **58**, 1028–1039 (2015).
26. M. K. Jang *et al.*, *Mol. Cell* **19**, 523–534 (2005).
27. Y. W. Jiang *et al.*, *Proc. Natl. Acad. Sci. U.S.A.* **95**, 8538–8543 (1998).
28. J. Lovén *et al.*, *Cell* **153**, 320–334 (2013).
29. S. Y. Wu, C. M. Chiang, *J. Biol. Chem.* **282**, 13141–13145 (2007).
30. A. S. Bhagwat *et al.*, *Cell Rep.* **15**, 519–530 (2016).

ACKNOWLEDGMENTS

We thank M. Adlanmerini, P. Dierickx, B. Fang, D. Guan, R. Papazyan, R. Soccio, Y. Aubert, and the Lazar laboratory for helpful discussions; J. Phillips-Cremins (University of Pennsylvania) and P. Huang and C. Edwards (Children's Hospital of Philadelphia) for technical advice; the Functional Genomics Core of the Penn Diabetes Research Center and the Penn Epigenetics Institute for next-generation sequencing; and the Viral Vector Core of the Penn Diabetes Research Center for recombinant virus preparation. ChIP-seq and Hi-C data have been deposited in the Gene Expression Omnibus (GSE104129). Supported by the JPB Foundation (M.A.L.) and by NIH grants R01 DK45586 and P30 DK19525 (M.A.L.), R01 DK106027 (K.-J.W.), and T32 GM007170, T32 GM008216, and F30 DK112507 (Y.H.K.).

SUPPLEMENTARY MATERIALS

www.sciencemag.org/content/359/6381/1274/suppl/DC1
Materials and Methods
Figs. S1 to S6
Tables S1 to S5
References (*31*–*35*)

18 August 2017; accepted 17 January 2018
Published online 8 February 2018
10.1126/science.aao6891

Science

Rev-erb# dynamically modulates chromatin looping to control circadian gene transcription

Yong Hoon KimSajid A. MarhonYuxiang ZhangDavid J. StegerKyoung-Jae WonMitchell A. Lazar

Science, 359 (6381), • DOI: 10.1126/science.aao6891

Chromosome dynamics and cellular clocks

Many genes undergo daily or circadian changes in their rate of transcription. Kim *et al.* explored the mechanism by which the circadian clock is linked to chromosome dynamics (see the Perspective by Diettrich Mallet de Lima and Göndör). They used a chromosome conformation capture technique (Hi-C) to identify the interactions of adjacent DNA fragments and determine how DNA looping that altered such interactions changed over daily cycles. The repressive transcription factor Rev-erb#, which functions as part of the mammalian clock mechanism, appears to bind to chromatin and recruit a protein complex that evicts other proteins that enhance looping, thus favoring enhancer-promoter interactions.

Science, this issue p. 1274; see also p. 1212

Science (ISSN 1095-9203) is published by the American Association for the Advancement of Science. 1200 New York Avenue NW, Washington, DC 20005. The title *Science* is a registered trademark of AAAS.